ELSEVIER

Thermodynamic treatment of noble metal fission products in nuclear fuel

M.H. Kaye, B.J. Lewis, W.T. Thompson *

Department of Chemistry and Chemical Engineering, Royal Military College of Canada, Kingston, Ont., Canada K7K 7B4

Abstract

Based on a critical evaluation of the literature, a comprehensive thermodynamic model has been developed for the complete quinary system involving the noble metal fission products in nuclear fuel: Mo–Pd–Rh–Ru–Tc. This treatment was based on the foundation of ten binary systems and an interpolation scheme. The thermodynamic model has been demonstrated to fit the available experimental data for the ternary sub-systems. This work can be used with other models for potentially non-stoichiometric UO_{2+x} containing fission products, as well as data for other phases, to assess the chemical form of fission products in irradiated fuel material.
© 2007 Elsevier B.V. All rights reserved.

1. Introduction

In nuclear reactor accidents, the behaviour of fission products is important in order to determine the potential for radioactive release. An understanding of the reaction of fission products with the surrounding system (e.g., the fuel and reactor structural components consisting of the Zircaloy cladding, primary heat transport system piping and containment vessel structure) is needed. An assessment of the chemical form is particularly needed to better predict the fission product release from the fuel (i.e., the source term) and their subsequent ability for transport in the primary heat transport system and retention behaviour in the containment [1–10].

Within the UO_2 fuel, it is known that the so-called 'noble metals' (i.e., Mo, Pd, Rh, Ru, and Tc) form white inclusions, first reported by Bramman et al. [11]. They observed that the five component alloy was in a hexagonal crystal structure, a result confirmed by O'Boyle et al. [12]. Fig. 1 schematically illustrates the noble metal inclusions among the various types of other secondary phases in the fuel oxide matrix [13].

A quantitative assessment of the oxygen potential is important to understand the fuel and fission product behaviour [14,15]. Various authors have shown that the noble metals give evidence of the oxygen potential of the system [16–18], but a complete thermodynamic treatment of the quinary alloy necessary to calculate the oxygen potential has not been reported. Instead, approximate treatments

* Corresponding author. Tel.: +1 613 544 6159; fax: +1 613 544 7900.
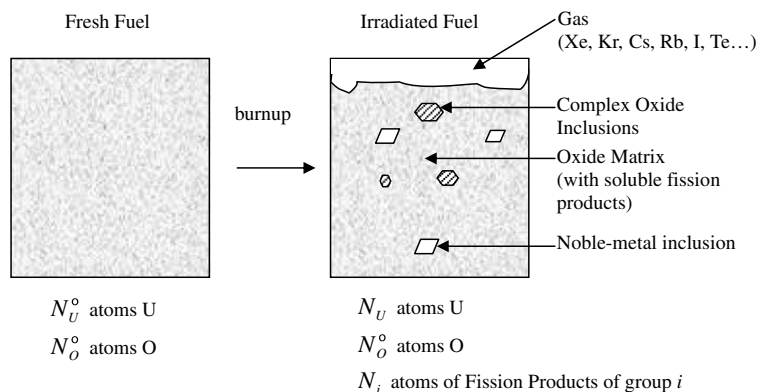 *E-mail address:* thompson-w@rmc.ca (W.T. Thompson).

Fig. 1. Typical result of irradiating fresh fuel [13].

have been suggested where the quinary is reduced to a 'suitable' pseudoternary. For example, in Matsui et al. [19] and Matsui and Naito [20], Ru represents both of the closed pack hexagonal (cph) elements (i.e., Ru and Tc) and Pd represents both of the face centered cubic (fcc) elements (i.e., Pd and Rh). Kleykamp et al. [21] adopt a similar strategy, with the fcc phase being 50 at.% Pd and 50 at.% Rh. Alternatively, Dwight and O'Boyle [22] suggest that the quinary can be treated as the Mo–Ru–Rh ternary.

To treat the complete Mo–Pd–Rh–Ru–Tc alloy system, it is necessary to model ten individual binary sub-systems. Five of these systems, Mo–Pd, Mo–Rh, Pd–Rh, Pd–Ru, and Rh–Ru have previously been evaluated [23–26]. These were reviewed for internal consistency and adjusted as required. To complete the quinary alloy system, the Mo–Ru binary system and the four binary systems involving Tc were critically assessed. The Mo–Ru system had been studied by various authors [27–32], while only limited data were available for the four Tc systems [33–40]. Once ten suitable models for the binary sub-systems had been assembled, interpolation into the higher-order systems was undertaken and compared to the limited experimental work available [41–45].

2. Thermodynamic modelling

2.1. Binary systems – previously assessed

Gibbs energy data from the literature for the evaluations of Mo–Pd; Mo–Rh; Pd–Rh; Pd–Ru; and Rh–Ru [23–26] have been accepted and are pre-sented here in Table 1 (lattice stabilities) and Table 2 (excess properties), where X_i is the mole fraction of element i and ΔG_j^E is the excess Gibbs energy for the specific condensed phase j.

2.1.1. Mo–Rh

In the Mo–Rh binary system, there are also 'low temperature' compounds that were outside the range of temperatures considered in the thermodynamic model of Gürler and Pratt [24]. For the compounds, MoRh and MoRh$_3$, which are stable to approximately 1323 K and 1470 K, respectively, the Gibbs energy of formation, ΔG°, used in the present treatment are given by Eqs. (1) and (2). Note that these equations refer to formation from components in the liquid state.

$$\Delta G^\circ_{\text{MoRh}} = -47\,100 + 16.7477T \text{ J mol}^{-1}$$
$$\text{(per 1/2 mol of MoRh)}, \tag{1}$$

$$\Delta G^\circ_{\text{MoRh}_3} = -503\,39.2 + 20T \text{ J mol}^{-1}$$
$$\text{(per 1/4 mol of MoRh}_3\text{)}. \tag{2}$$

The updated Mo–Rh phase diagram, which includes these two compounds, is shown in Fig. 2. The positions of the eutectoid tielines (at 1273 K and 1423 K) agree with the diagram for the Mo–Rh system published in the Bulletin of Alloy Phase Diagrams (BAPD) [39], reproduced here (with permission) as Fig. 3.

2.1.2. Pd–Rh

In the Pd–Rh system, experimental data along the solidus and liquidus are scarce in the literature. Differential Thermal Analysis (DTA) measurements were performed to clarify their position, the details

Table 1
Lattice stabilities for the components

Phase	Gibbs energy for the lattice stability (J mol^{-1})	Comment	Reference
$G°$ (Mo,liquid)	0	Reference phase	
$G°$ (Mo,bcc)	$-41\,403 + 14.30 \cdot T$		[23,24]
$G°$ (Mo,cph)	$-29\,853 + 14.30 \cdot T$	Hypothetical	[23,24]
$G°$ (Mo,fcc)	$-26\,203 + 14.93 \cdot T$	Hypothetical	[23,24]
$G°$ (Pd,liquid)	0	Reference phase	
$G°$ (Pd,bcc)	$-12\,300 + 12.37 \cdot T$	Hypothetical	[23]
$G°$ (Pd,cph)	$-12\,300 + 14.88 \cdot T$	Hypothetical	[23,26,32]
$G°$ (Pd,fcc)	$-16\,480 + 9.02 \cdot T$		[23,25,26,32]
$G°$ (Rh,liquid)	0	Reference phase	
$G°$ (Rh,bcc)	$-19\,664 + 16.27 \cdot T$	Hypothetical	[24]
$G°$ (Rh,cph)	$-25\,910 + 12.51 \cdot T$	Hypothetical	[24,26]
$G°$ (Rh,fcc)	$-26\,568 + 11.88 \cdot T$		[24–26]
$G°$ (Ru,liquid)	0	Reference phase	
$G°$ (Ru,bcc)	$-30\,420 + 12.51 \cdot T$	Hypothetical	[32]
$G°$ (Ru,cph)	$-38\,589 + 14.80 \cdot T$		[26]
$G°$ (Ru,fcc)	$-21\,019 + 8.94 \cdot T$	Hypothetical	[26,32]
$G°$ (Tc,liquid)	0	Reference phase	
$G°$ (Tc,bcc)	$-28\,000 + 12.00 \cdot T$	Hypothetical	
$G°$ (Tc,cph)	$-33\,290 + 13.44 \cdot T$		[39,40]
$G°$ (Tc,fcc)	$-30\,000 + 14.00 \cdot T$	Hypothetical	
$G°$ (Tc,tetra)	$-20\,000 + 13.50 \cdot T$	Hypothetical	

Table 2
Excess properties[a] for the binary subsystems [23–26]

Phase	Binary	Expression for the excess Gibbs energy (i.e., ΔG^E) (J mol^1)
L	Mo–Pd	$\Delta G^E_{Liquid} = X_{Mo}X_{Pd}[366\,904.56 - 478\,773X_{Pd} - (193.12 - 216.85X_{Pd})T]$
bcc	Mo–Pd	$\Delta G^E_{bcc} = X_{Mo}X_{Pd}[40\,328.63 + 1\,220\,269X_{Pd} - (73.49 + 159.92X_{Pd})T]$
cph	Mo–Pd	$\Delta G^E_{cph} = X_{Mo}X_{Pd}[11\,387.07 + 656.46X_{Pd} - (16.81 + 53.33X_{Pd})T]$
fcc	Mo–Pd	$\Delta G^E_{fcc} = X_{Mo}X_{Pd}[71\,076.50 - 100\,416.81X_{Pd} - (50.59 - 27.84X_{Pd})T]$
L	Mo–Rh	$\Delta G^E_{Liquid} = X_{Mo}X_{Rh}\begin{bmatrix} -60\,261.04 - 84\,654.63X_{Rh} - 27.78X_{Rh}^2 \\ -(18.39 - 44.14X_{Rh} - 0.22X_{Rh}^2)T \end{bmatrix}$
bcc	Mo–Rh	$\Delta G^E_{bcc} = X_{Mo}X_{Rh}[22\,507.43 - 41\,776.92X_{Rh} - (5.48 + 7.67X_{Rh})T]$
cph	Mo–Rh	$\Delta G^E_{cph} = X_{Mo}X_{Rh}[-8453.152 - 60\,006.5X_{Rh} - (5.495 - 25.872X_{Rh})T]$
fcc	Mo–Rh	$\Delta G^E_{fcc} = X_{Mo}X_{Rh}[110\,113.559 - 199\,401.5X_{Rh} - (65.004 - 99.42X_{Rh})T]$
L	Pd–Rh	$\Delta G^E_{Liquid} = X_{Pd}X_{Rh}[20\,027 - 2260X_{Rh} - (2.74 - 0.56X_{Rh})T]$
bcc	Pd–Rh	$\Delta G^E_{bcc} = X_{Pd}X_{Rh}[20\,920]$ (hypothetical)
cph	Pd–Rh	$\Delta G^E_{cph} = X_{Pd}X_{Rh}[20\,920]$ (hypothetical)
fcc	Pd–Rh	$\Delta G^E_{fcc} = X_{Pd}X_{Rh}[21\,247 + 2199X_{Rh} - (2.74 - 0.56X_{Rh})T]$
L	Pd–Ru	$\Delta G^E_{Liquid} = X_{Pd}X_{Ru}[187\,564.062 - 62\,169.281X_{Pd} - (63.661 - 6.64X_{Pd})T]$
bcc	Pd–Ru	$\Delta G^E_{bcc} = X_{Pd}X_{Ru}[20\,000]$ (hypothetical)
cph	Pd–Ru	$\Delta G^E_{cph} = X_{Pd}X_{Ru}[-1524.818 + 14.933T]$
fcc	Pd–Ru	$\Delta G^E_{fcc} = X_{Pd}X_{Ru}[-5049.035 + 17.59T]$
L	Rh–Ru	$\Delta G^E_{Liquid} = X_{Rh}X_{Ru}[-35\,739.32 + 16.369T]$
bcc	Rh–Ru	$\Delta G^E_{bcc} = 0$ (hypothetical)
cph	Rh–Ru	$\Delta G^E_{cph} = X_{Rh}X_{Ru}[-26\,440.004 + 10.445T]$
fcc	Rh–Ru	$\Delta G^E_{fcc} = X_{Rh}X_{Ru}[-53\,477.07 + 21.738T]$

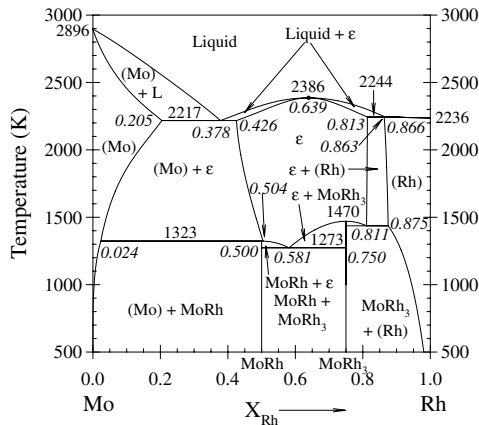[a] Excess properties of four hypothetical phases added by the authors.

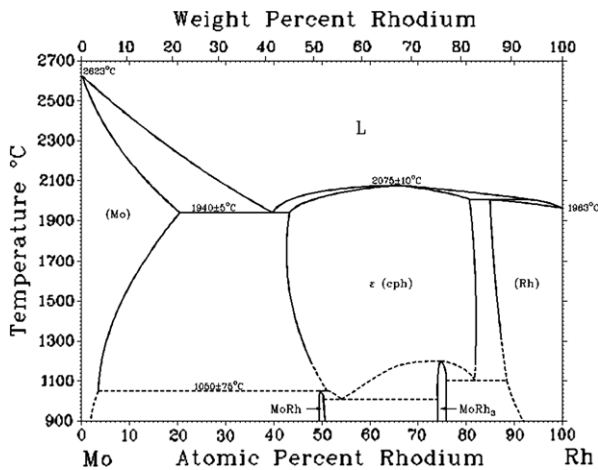Fig. 2. The amended evaluation of the Mo–Rh system including MoRh and MoRh$_3$.

Fig. 3. The Mo–Rh system as published in the Bulletin of Alloy Phase Diagrams [39] (used with permission).
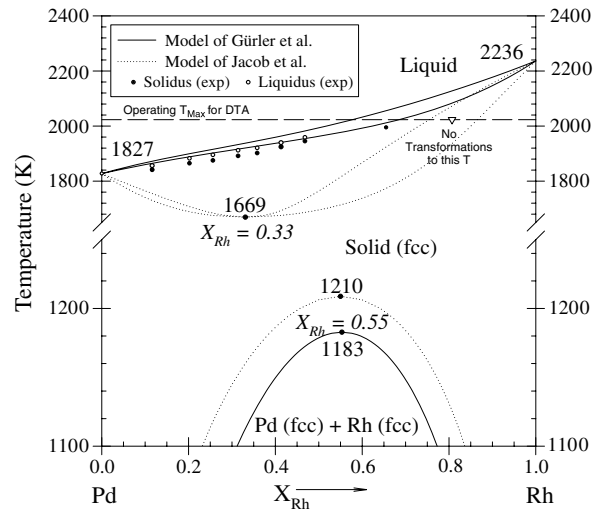

Fig. 4. The evaluation of the Pd–Rh system by Gürler et al. [25] (solid lines) compared to that proposed by Jacob et al. [47] (dotted lines). The experimental data from the present DTA work are also shown.

of which are reported elsewhere [46]. Recent emf measurements by Jacob et al. [47], confirmed the placement of the solid miscibility gap, previously reported [48–50] and modelled by Gürler et al. [25], shown in Fig. 4. Jacob et al. [47] proposed an ideal liquid solution, which differs from the treatment by Gürler et al. [25]. Also shown in Fig. 4, are the current experimental data, which support the solidus and liquidus proposed by Gürler et al. [25].

2.2. Binary systems – not previously modelled

Thermodynamic treatments for Mo–Ru, Mo–Tc, Pd–Tc, Rh–Tc, and Ru–Tc are needed to complete the noble metal quinary system. Of these five sys-

tems, the Mo–Ru binary has been studied the most and so greater attention will be given here to it. Because experimental data in systems involving Tc have been difficult to obtain, the available literature for these systems is much less, but nonetheless what little that is available has been used to construct four thermodynamic treatments that satisfy the available data.

The thermodynamic data for all five treatments are summarized in Table 3. The Gibbs energy of formation, $\Delta G°$, for the two compounds Mo$_5$Ru$_3$ and Mo$_9$Tc$_{11}$ are given by Eqs. (3) and (4), respectively.

$$\Delta G°_{Mo_5Ru_3} = 4430 - 7.68495T \text{ J mol}^{-1}$$
$$(\text{per } \frac{1}{8} \text{mol of Mo}_5\text{Ru}_3), \tag{3}$$

$$\Delta G°_{Mo_9Tc_{11}} = [-42794.3 + 13.8253T] \text{J mol}^{-1}$$
$$(\text{per } \frac{1}{20} \text{ mol Mo}_9\text{Tc}_{11}). \tag{4}$$

For Eq. (3), the reference states are the solids, Mo$_{(bcc)}$ and Ru$_{(cph)}$, while Eq. (4) refers to formation from components in their liquid states (i.e., Mo$_{(liq)}$ and Tc$_{(liq)}$).

2.2.1. Mo–Ru

The X–ray diffraction and metallographic studies of Anderson and Hume-Rothery [27] established the presence of the four condensed phases and positioned the intermediate tetragonal compound as

Table 3
Excess properties for binary subsystems, supplementary to Table 2

Phase	Binary	Expression for the excess Gibbs energy (i.e., ΔG^{E}) (J mol^{1})
L	Mo–Ru	$\Delta G^{\text{E}}_{\text{Liquid}} = X_{\text{Mo}}X_{\text{Ru}}[-46\,277 + 26\,370X_{\text{Ru}}]$
bcc	Mo–Ru	$\Delta G^{\text{E}}_{\text{bcc}} = X_{\text{Mo}}X_{\text{Ru}}[33\,863 + 730.47X_{\text{Ru}} - 18.335T]$
cph	Mo–Ru	$\Delta G^{\text{E}}_{\text{cph}} = X_{\text{Mo}}X_{\text{Ru}}[78\,174 - 169\,180X_{\text{Ru}} - (50 - 80X_{\text{Ru}})T]$
fcc	Mo–Ru	$\Delta G^{\text{E}}_{\text{fcc}} = X_{\text{Mo}}X_{\text{Ru}}[15\,000]$
L	Mo–Tc	$\Delta G^{\text{E}}_{\text{Liquid}} = X_{\text{Mo}}X_{\text{Tc}}[-4904.1 + 21\,680X_{\text{Tc}}]$
bcc	Mo–Tc	$\Delta G^{\text{E}}_{\text{bcc}} = X_{\text{Mo}}X_{\text{Tc}}[-3882.8 - 21\,442X_{\text{Tc}} + (11 + 11X_{\text{Tc}})T]$
cph	Mo–Tc	$\Delta G^{\text{E}}_{\text{cph}} = X_{\text{Mo}}X_{\text{Tc}}[59\,650 + 27\,437X_{\text{Tc}} - (20 + 10X_{\text{Tc}})T]$
tetra	Mo–Tc	$\Delta G^{\text{E}}_{\text{tetragonal}} = X_{\text{Mo}}X_{\text{Tc}}[-28\,106 - 150\,380X_{\text{Tc}} - (10 - 50X_{\text{Tc}})T]$
L	Pd–Tc	$\Delta G^{\text{E}}_{\text{Liquid}} = X_{\text{Pd}}X_{\text{Tc}}[187\,564 - 62\,169.3X_{\text{Pd}} - (63.661 - 6.64X_{\text{Pd}})T]$
bcc	Pd–Tc	$\Delta G^{\text{E}}_{\text{bcc}} = X_{\text{Pd}}X_{\text{Tc}}[20\,000 + 0T]$
cph	Pd–Tc	$\Delta G^{\text{E}}_{\text{cph}} = X_{\text{Pd}}X_{\text{Tc}}[-5962.7 + 4296X_{\text{Tc}} - (12.92 - 27.13X_{\text{Tc}})T]$
fcc	Pd–Tc	$\Delta G^{\text{E}}_{\text{fcc}} = X_{\text{Pd}}X_{\text{Tc}}[-500 + 12T]$
L	Rh–Tc	$\Delta G^{\text{E}}_{\text{Liquid}} = X_{\text{Rh}}X_{\text{Tc}}[293\,000 - 131\,000X_{\text{Tc}} - (113.54 - 43.75X_{\text{Tc}})T]$
bcc	Rh–Tc	$\Delta G^{\text{E}}_{\text{bcc}} = 0$
cph	Rh–Tc	$\Delta G^{\text{E}}_{\text{cph}} = X_{\text{Rh}}X_{\text{Tc}}[-28\,250 - 111\,959X_{\text{Tc}} + (21.28 + 28.94X_{\text{Tc}})T]$
fcc	Rh–Tc	$\Delta G^{\text{E}}_{\text{fcc}} = X_{\text{Rh}}X_{\text{Tc}}[-9562.8 + 16T]$
All	Ru–Tc	All excess properties assumed to be 0
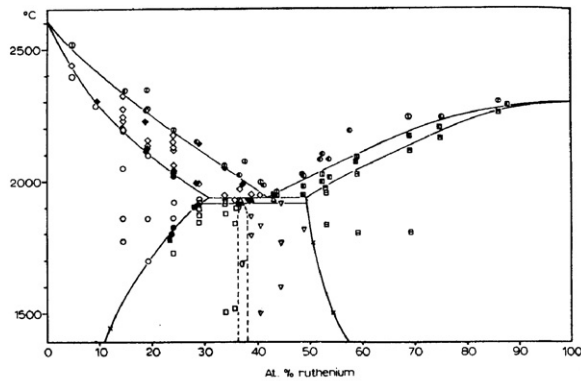
Molybdenum–ruthenium equilibrium diagram. × refer to X-ray points. The full points refer to specimens analysed after the experiments. For the open points, the compositions are either taken to be the same as the analytical values for another specimen of the same bar, or are the synthetic values: ○, α–Mo; ◑, quenched liquid; ◊, α–Mo + liquid; □, α–Mo + σ; ⊟, α–Ru; ◫, α–Ru + liquid; ◇, α–Ru + σ; △, α–Mo + α–Ru.

Fig. 5. Mo–Ru equilibrium diagram from Anderson and Hume-Rothery [27] (used with permission).

stoichiometric Mo$_5$Ru$_3$. Since all their data applied to temperatures above 1673 K, the proposed diagram, Fig. 5, suggests stability for the σ-phase below 1900 °C. Kieffer and Sedlatschek [28] generally confirmed this but their proposed diagram differed in two details: the tetragonal σ-phase was positioned at Mo$_3$Ru$_2$; and the σ-phase had a stability range limited in temperature from ~1260 to

1850 °C. An experimental examination by Kleykamp [29–31] confirmed the diagram and established the eutectic transformation at 2228 ± 10 K, a peritectoid transformation at 2188 K, and a eutectoid transformation at 1416 K [29].

Rand and Potter [32] based their modelling on previously determined experimental features. They treated the σ-phase as a stoichiometric compound

with the composition Mo_5Ru_3. The solidus and liquidus did not provide a narrow two-phase region as suggested by experimental results. However, the parameters derived for this model were not published [32].

An experimental examination of the Mo–Ru binary system was undertaken by Kleykamp [29–31], using metallography, X–ray diffraction, and DTA to establish phase boundaries. Electrochemical methods were also used to measure thermodynamic properties.

By using DTA, Kleykamp established that the eutectic temperature in this system was 2228 ± 10 K. Also using DTA and dilatometry, the peritectoid and eutectoid reactions that involve bcc-solid rich Mo, cph-solid rich Ru, and σ-phases, were determined to occur at 2188 K and 1416 K, respectively [29]. Results from the X-ray microanalysis (XMA) of a series of alloys heat treated at various temperatures, were used to graphically determine the solvus boundaries in the Mo–Ru system [29].

Using the solid galvanic cell schematically shown in Eq. (5), the relative partial molar Gibbs energy of molybdenum in the Mo–Ru system was measured from 1150 to 1350 K.

$$(-)Re|Fe,FeO_{0.95}|Zr(Ca)O_2|MoO_2,Mo–Ru\ alloy|Re(+) \tag{5}$$
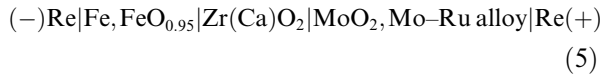
The relative partial molar excess Gibbs energy $(\Delta \overline{G}^E)$ of molybdenum with respect to bcc-Mo at infinite dilution in ruthenium was reported as follows: at 1200 K, $\Delta \overline{G}^E_{Mo,\ w.r.t.\ bcc} = -43$ kJ mol^{-1}, and at 1300 K, $\Delta \overline{G}^E_{Mo,\ w.r.t.\ bcc} = -40$ kJ mol^{-1}.

For the current purpose, the lattice stabilities, $G°$ (with respect to liquid), for molybdenum and ruthenium are given in Table 1. For the hypothetical crystal structures, values were taken to agree with previous evaluations [23,24,26,32]. The excess properties of mixing, ΔG^E, for the solution phases are given in Table 3. As mentioned previously, Kleykamp provided partial molar excess Gibbs energies at infinite dilution of Mo in cph–Ru solid solution [29,30]. The partial molar excess Gibbs energy for Mo with respect to cph–solid is given by

$$\Delta \overline{G}^E_{Mo,\ w.r.t.\ cph} = X_{Ru}^2[247354 - 338360X_{Ru} \\ - (130 - 160X_{Ru})T]\ \text{J mol}^{-1}. \tag{6}$$

At infinite dilution of Mo, $X_{Ru} = 1$, and (6) simplifies to

$$\Delta \overline{G}^E_{Mo,\ w.r.t.\ cph} = [-91006 + 30T]\ \text{J mol}^{-1} \tag{7}$$

Kleykamp reported that at 1200 K and 1300 K $\Delta \overline{G}^E_{Mo,\ w.r.t.\ bcc} = -43$ kJ mol^{-1} and -40 kJ mol^{-1}, respectively [31]. By solving (7) and using the difference in Gibbs energy from Table 1 to convert from the cph-solid reference state to the bcc-solid reference state (i.e., $+11550$ J mol^{-1}), values of $\Delta \overline{G}^E_{Mo,\ w.r.t.\ bcc} = -43.46$ kJ mol^{-1} and -40.46 kJ mol^{-1}, at 1200 K and 1300 K, may be obtained to give evidence of consistency with the measurements of Kleykamp.

2.2.1.1. Properties of Mo_5Ru_3. To model the behaviour of the compound Mo_5Ru_3, it is necessary to have the standard enthalpy at 298.15 K, $\Delta H°_{298}$, and the standard entropy at 298.15 K, $S°_{298}$. These values were chosen as: $\Delta H°_{298} = 35440$ J mol^{-1} and $S°_{298} = 290.1092$ J K^{-1} mol^{-1}. The heat capacity, C_p, was determined to be: $C_p = 221.0131 - 0.02404T - 2548550 \times T^{-2} + 3.05593 \times 10^{-5}T^2$ J K^{-1} per mol Mo_5Ru_3. The C_p expression for Mo_5Ru_3 was taken to be

$$C_{pMo_5Ru_3} = 5C_{pMo_{(bcc)}} + 3C_{pRu_{(cph)}}. \tag{8}$$

The expression $\Delta G°_{Mo_5Ru_3} = 4430 - 7.68495T$ J per $\frac{1}{8}$ mol of Mo_5Ru_3 (with respect to $Mo_{(bcc)}$ and $Ru_{(cph)}$) was used to establish $\Delta H°_{298}$ and $S°_{298}$. For $\Delta H°_{298}$, the following was used:

$$\Delta H°_{298} = 8(4430) = 35440\ \text{J mol}^{-1}_{Mo_5Ru_3}. \tag{9}$$

For $S°_{298}$ the relationships expressed in (10) and summed in (11) were used.

$$\Delta S°_{298\ Mo_5Ru_3} = S°_{298\ Mo_5Ru_3} - 5S°_{298\ Mo} - 3S°_{298\ Ru} \tag{10}$$

$$S°_{298\ Mo_5Ru_3} = 8(7.68495) + 5(28.605) \\ + 3(28.53488) = 290.1092\ \text{J K}^{-1}\ \text{mol}^{-1}_{Mo_5Ru_3} \tag{11}$$

The computed Mo–Ru phase diagram resulting from the foregoing thermodynamic data is shown in Fig. 6 in relation to the data of Kleykamp [29–31]. Fig. 7 shows the same computed diagram in relation to the work of Anderson and Hume-Rothery [27].

Details of the computed invariant temperatures and co-existent phase compositions, difficult to resolve in Figs. 6 and 7, are given in Table 4.

Experimental data of Gürler [51] support the position of the solvus boundaries below the eutectoid temperature, 1416 K. A comparison of the solvus compositions is made in Table 5 [51].
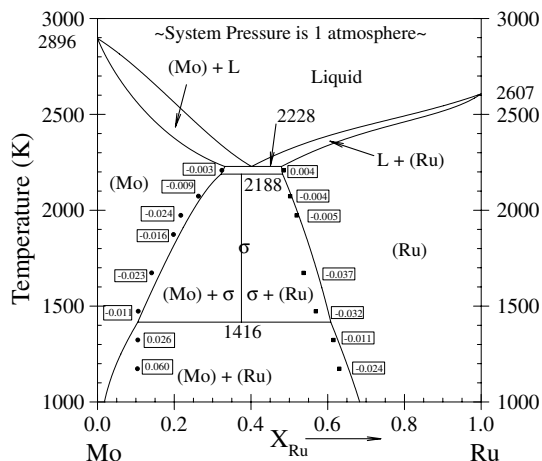
Fig. 6. Comparison of the data of Kleykamp [29–31] with the modelled phase diagram. The boxed values represent the difference between the data of Kleykamp and the values computed with the proposed treatment.
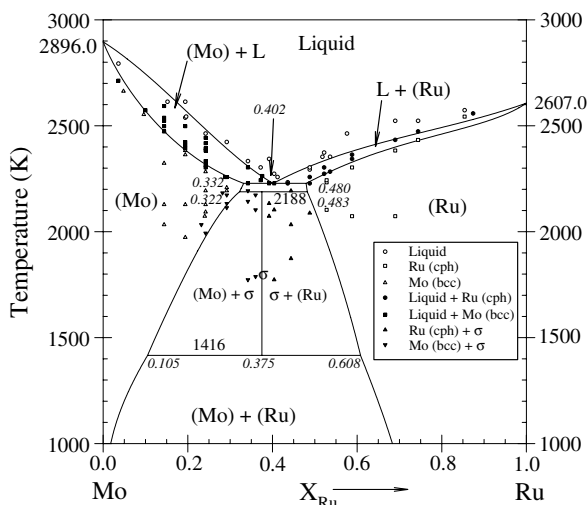

Fig. 7. Comparison of experimental work of Anderson and Hume-Rothery [27] with the current treatment of the Mo–Ru system.

2.2.2. Mo–Tc

Of the four binary systems that involve technetium, the Mo–Tc binary system has been investigated the most and is also the most complex, since at least four solid phases have been identified. The first study, by Compton et al. [33], was concerned with determining the superconductivity properties of Mo–Tc alloys at extremely low temperatures. Darby et al. [34,35] reported the first crystallographic data for eleven alloys annealed at temperatures between 773 K and 1323 K. Using X-ray

diffraction they found that four solid phases existed, namely: a Mo-rich bcc-solid (β); a cP8 structure (κ)[1]; a σ-phase (tetragonal phase); and a Tc-rich cph-solid (ε). The composition, X_{Tc}, in atomic percent, of the cP8 structure was determined to lie within the narrow range of 54 ± 2 at.% Tc. Specifically, the intermediate cubic structure must lie between $0.50 < X_{Tc} < 0.56$ at 873 K, and a narrower range of $0.53 < X_{Tc} < 0.56$ at 1323 K. The σ-phase, however, was found to have a wide compositional range that centered about 70 at.% Tc. At 973 K the boundary between σ and the $\sigma + \varepsilon$ two phase region was found to be between 75 and 77 at.% Tc. The boundary between the σ and the $\sigma + \kappa$ two phase region was less well defined, lying between 60 and 70 at.% Tc at 973 K.

The summary of molybdenum phase diagrams prepared by Brewer [52] reported the presence of five phases: the liquid, a terminal Mo-rich bcc phase extending to $X_{Tc} \approx 0.50$, a terminal Tc-rich cph phase extending to $X_{Tc} \approx 0.85$, an intermediate tetragonal phase centered at $X_{Tc} = 0.70$, and another intermediate cubic solid at $X_{Tc} = 0.55$. The equilibrium phase diagram proposed by Brewer [39] is shown Fig. 8.

Because the phase diagrams involving Tc and the other noble metals were being added to the existing Mo–Pd–Rh–Ru quaternary system to produce a complete quinary system, the lattice stabilities for the existing quaternary must be used in order to guarantee consistency in the modelling process. These lattice stabilities are summarized in Table 1. The excess properties of mixing, ΔG^E, for the solution phases are given in Table 3.

The Mo–Tc treatment was developed by considering data suggested by Brewer [52]. His attempt to define the liquidus over the complete compositional range was unsuccessful, but he suggested representing the thermodynamic behaviour of the liquid for $0 \leqslant X_{Tc} \leqslant 0.67$ in terms of the activity coefficients, γ_{Mo} and γ_{Tc}, which are functions of composition and temperature, by

$$\ln \gamma_{Mo} = X_{Tc}^2 \left(\frac{100}{T} - 400 X_{Tc} \right), \tag{12}$$

and

$$\ln \gamma_{Tc} = X_{Mo}^2 \left(\frac{-500}{T} + \frac{400 X_{Mo}}{T} \right) + \frac{50}{T} \tag{13}$$

---

[1] Reported as an A15–Cr$_3$O type simple cubic structure by Darby and Zegler [34].

Table 4
Invariant points on the modelled Mo–Ru phase diagram

Reaction	Composition of the respective phases, at.% Ru			T (K)	T (°C)	Type
L ↔ Mo		0		2896	2623	Melting
L ↔ (Mo) + (Ru)	33.2	40.2	48.0	2228	1955	Eutectic
(Mo) + (Ru) ↔ σ	32.2	37.5	48.3	2188	1915	Peritectoid
σ ↔ (Mo) + (Ru)	10.5	37.5	60.8	1416	1143	Eutectoid
L ↔ Ru		100.0		2607	2334	Melting

Table 5
Comparison of solvus compositions from Gürler [51] and this work

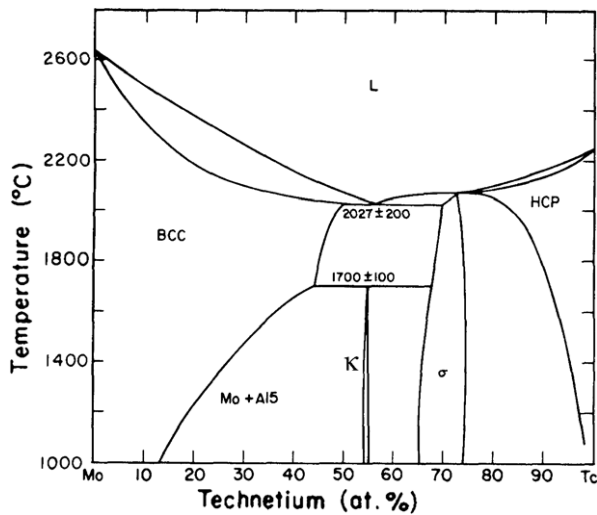| Temperature (K)	bcc Solvus from Gürler (at.% Ru)	bcc Solvus this work (at.% Ru)	cph Solvus from Gürler (at.% Ru)	cph Solvus this work (at.% Ru)
973	2.90	1.51	64.1	68.8
1073	3.25	2.72	63.5	67.2
1173	3.60	4.43	62.8	65.4
1223	3.75	5.47	62.2	64.5
1323	4.40	7.90	61.2	62.6
1388	5.25	9.69	60.4	61.4
1473	7.90	11.74	59.3	60.1

Fig. 8. Mo–Tc equilibrium diagram from Brewer [39,52] (used with permission).

while for $0.67 \leqslant X_{Tc} \leqslant 1$, the liquid behaviour was defined by

$$\ln \gamma_{Mo} = X_{Tc}^2 \left(\frac{-325}{T} + \frac{350 X_{Tc}}{T} \right) - \frac{33}{T} \quad (14)$$

and

$$\ln \gamma_{Tc} = X_{Mo}^2 \left(\frac{200}{T} - \frac{350 X_{Mo}}{T} \right). \quad (15)$$

By considering these four equations, the critical temperatures and compositions for the eutectic and eutectoid reactions, and the experimentally determined solubility limits for the σ-solid phase, it was possible to mathematically determine the equilibrium phase diagram. In this computation the intermediate cubic structure, κ, was treated as a stoichiometric compound, Mo_9Tc_{11}. For the compound, κ, Mo_9Tc_{11}, the Gibbs energy of formation, $\Delta G^{\circ}_{Mo_9Tc_{11}}$, was

$$\Delta G^{\circ}_{Mo_9Tc_{11}} = [-42794.3 + 13.8253T] \text{ J mol}^{-1}$$

$$\text{per } \frac{1}{20} \text{ mol } Mo_9Tc_{11}. \quad (16)$$

Eq. (16) refers to the formation from molybdenum and technetium in their liquid states (i.e., $Mo_{(liq)}$ and $Tc_{(liq)}$). The Mo–Tc phase diagram developed is shown in Fig. 9. This diagram respects the compositional requirements suggested by Darby et al. [34,35] at 873 K and 973 K.

The invariant points for the computed diagram for Mo–Tc are assembled in Table 6.

2.2.3. Pd–Tc

Experimental work in the Pd–Tc system has been very limited. It was speculated by Ageev et al. [36] and verified by others (e.g., Compton et al. [33] and Darby et al. [35]) that the alloying behaviour of rhenium and technetium would be similar, as they are both Group VIIB elements (i.e., the Mn
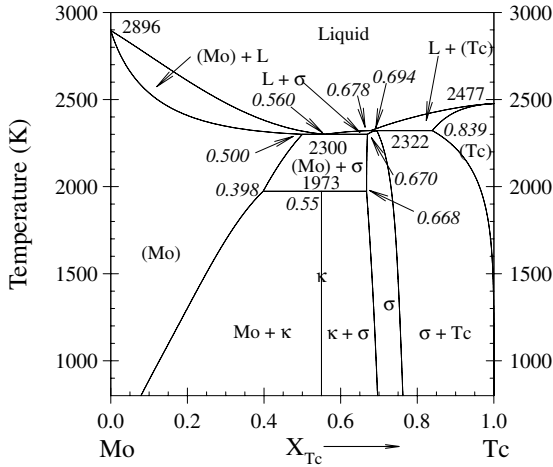
Fig. 9. The computed Mo–Tc system.

Gibbs energy expressions for the fcc-solid phase and cph-solid phase were developed from limited data. A tie line between the fcc-solid and the cph-solid at 1773 K, which satisfied the given data, was extended from the fcc-solid boundary at $X_{Pd} \cong 0.73$ and the cph-solid boundary at $X_{Pd} \cong 0.49$. At 1323 K another tie line, which satisfied the data, was extended from the fcc-solid boundary at $X_{Pd} \cong 0.25$ and the cph-solid boundary at $X_{Pd} \cong 0.47$. At every temperature along a tie line the partial Gibbs energy of palladium, $\overline{G}_{Pd}$, in the fcc-solid and cph-solid are equal, therefore:

$$\overline{G}_{Pd}^{fcc} = \overline{G}_{Pd}^{cph} \tag{17}$$

and

$$\overline{G}_{Tc}^{fcc} = \overline{G}_{Tc}^{cph}. \tag{18}$$

Eq. (17) is equivalent to

$$\left(\overline{G}_{Pd}^{fcc} - G_{Pd}^{\circ fcc}\right) = \left(\overline{G}_{Pd}^{cph} - G_{Pd}^{\circ cph}\right) + \left(G_{Pd}^{\circ cph} - G_{Pd}^{\circ fcc}\right) \tag{19}$$

and Eq. (18) is equivalent to

$$\left(\overline{G}_{Tc}^{fcc} - G_{Tc}^{\circ fcc}\right) = \left(\overline{G}_{Tc}^{cph} - G_{Tc}^{\circ cph}\right) + \left(G_{Tc}^{\circ cph} - G_{Tc}^{\circ fcc}\right). \tag{20}$$

Each of the bracketed expressions was rearranged further. The first two expressions in Eq. (19) are equivalent to $RT \ln a_{Pd}$ in the particular phase, where R is the universal gas constant and a_{Pd} is the activity of Pd. The third expression is simply the difference in the lattice stabilities of the two different phases. Because $a_{Pd} = (X_{Pd}) \cdot (\gamma_{Pd})$, Eq. (19) was rewritten as

$$RT \ln X_{Pd}^{fcc} + \overline{G}_{Pd}^{Efcc} = RT \ln X_{Pd}^{cph} + \overline{G}_{Pd}^{Ecph} + \left(G_{Pd}^{\circ cph} - G_{Pd}^{\circ fcc}\right). \tag{21}$$

group). Because of this similarity, it is speculated that the system will exhibit a peritectic reaction. It should be noted that Pd has a tendency to this behaviour with other hexagonal transition metals (e.g., Pd–Ru, Pd–Os, and Pd–Re [39]). In 1962, Darby et al. [37] studied the system by examining, with X-ray metallography, alloys that had previously been annealed for 7 days at 1323 K. The results suggested that the maximum compositional variation for the mixture of terminal fcc-Pd and terminal cph-Tc lay in the range $0.5 < X_{Pd} < 0.75$. Furthermore, two phases were identified at $X_{Pd} = 0.666$. A similar study in 1963 by Niemiec [38] examined alloys that were annealed for 20 h at 1773 K. From this work, the solvus between the terminal fcc-Pd and the two phase region must lie in the range $0.684 < X_{Pd} < 0.75$, approximately at $X_{Pd} = 0.73$. For the solvus between the terminal cph-Tc and the two phase mixture, the boundary must lie between $0.47 < X_{Pd} < 0.565$, approximately at $X_{Pd} = 0.49$.

The current published diagram [39] is presented in Fig. 10.

Table 6
Invariant points on the computed Mo–Tc phase diagram

Reaction	Composition of the respective phases, at.% Tc			T (K)	T (°C)	Type
L ↔ Mo		0		2896	2623	Melting
L + (Tc) ↔ σ	67.8	69.4	83.9	2322	2049	Peritectic
L ↔ (Mo) + σ	50.0	56.0	67.0	2300	2027	Eutectic
(Mo) + σ ↔ κ	39.8	55.0	66.8	1973	1700	Peritectoid
L ↔ Tc		100.0		2477	2204	Melting
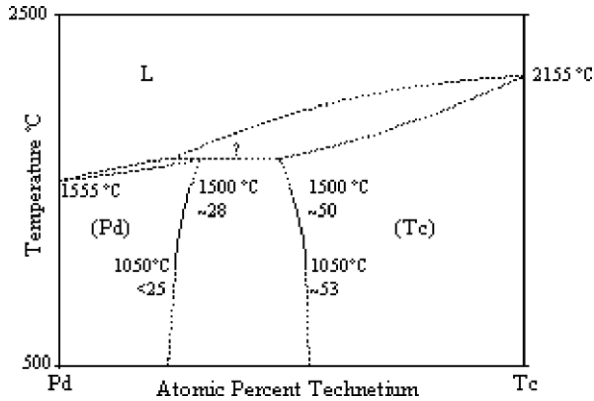
Fig. 10. Pd–Tc equilibrium diagram [39] (used with permission).

Fig. 11. Comparison of Pd–Tc phase diagram as evaluated for this work with experimental data from Darby et al. [37] and Niemiec [38].
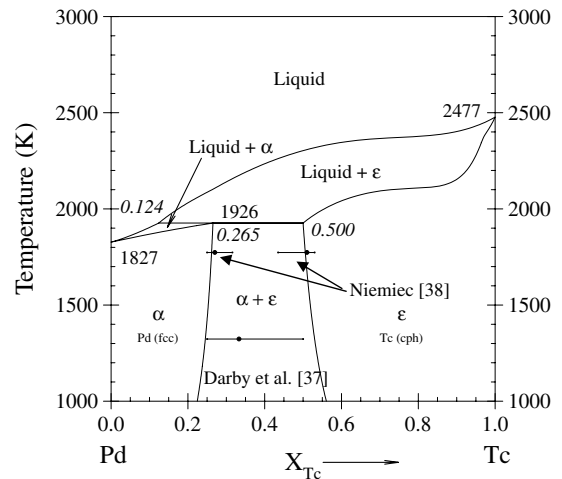
The Margules formalism [53] was used to represent the partial excess Gibbs energy term. By only considering the first two terms in the recursion relationship and then allowing for a temperature dependence for each of these terms, it is possible, given two tie-lines at distinct temperatures to solve for all the parameters. In this manner, the excess Gibbs energy expressions were developed for both the fcc-solid and the cph-solid. Once tentative Gibbs energy expressions for the two solids had been determined, the liquid phase was introduced in a similar manner. Finally, fine adjustments to all the constants in the excess Gibbs energy expressions for some or all of the phases were made to better represent the overall features of the equilibrium phase diagram (e.g., an appropriate peritectic temperature). The excess Gibbs energies for the solution phases are given in Table 3. Note that the excess Gibbs energy for the bcc-solid phase required a positive term (instead of 0) to prevent the phase becoming stable at high temperatures. A comparison of the current evaluation with the experimental work of Darby et al. [37] and Niemiec [38] is shown in Fig. 11. The diagram is consistent with the limited experimental work. The position of the two phase region at 1323 K suggested by Darby et al. [37] is respected. Furthermore, the boundaries proposed by Niemiec [38] at 1773 K are also respected.

A comparison of the computed phase diagram in Fig. 11, and the published diagram in Fig. 10, reveals a discrepancy between the solidus and liquidus lines as they approach the melting temperature of Tc. The solidus and liquidus compositions are related by

$$(RT \ln X_{\mathrm{Tc}}^{\mathrm{Liquid}}) = (RT \ln X_{\mathrm{Tc}}^{\mathrm{Solid}}) + (\Delta H_{\mathrm{Tc}}^{\mathrm{Melt}} - T\Delta S_{\mathrm{Tc}}^{\mathrm{Melt}}).$$
(22)

where R represents the gas constant, T the temperature of interest, $X_{\mathrm{Tc}}^{\mathrm{Liquid}}$ the mole fraction of Tc at the liquidus, and $X_{\mathrm{Tc}}^{\mathrm{Solid}}$ the mole fraction of Tc at the solidus. The dotted construction in Fig. 10 cannot be brought into accord with the enthalpy (or entropy) of melting, and is therefore thought to be erroneous.

2.2.4. Rh–Tc

Experimental work in the Rh–Tc system has also been limited. Darby et al. [37] studied the system by examining, with X-ray metallography, alloys that had previously been annealed for 7 days at 1323 K. The results suggested that the maximum compositional variation for the mixture of terminal fcc-Rh and terminal cph-Tc lay in the range $0.5 < X_{\mathrm{Rh}} < 1$. Furthermore, at $X_{\mathrm{Rh}} = 0.75$, only a trace of the fcc-Rh phase was detected, suggesting that the solvus boundary between the cph-Tc phase and the two phase region was at a composition range of $0.65 < X_{\mathrm{Rh}} < 0.75$. A similar study in 1963 by Niemiec [38] studied alloys that were annealed for 20 h at 1773 K. From this work, the solvus between the terminal fcc-Rh and the two phase region must lie in the range $0.955 < X_{\mathrm{Rh}}$, approximately at $X_{\mathrm{Rh}} = 0.98$. For the solvus between the terminal cph-Tc and the two phase mixture, the boundary must lie between $0.658 < X_{\mathrm{Rh}} < 0.763$, approximately at $X_{\mathrm{Rh}} = 0.70$. The current published diagram [39] is presented in Fig. 12.

There were limited experimental data on which to base a thermodynamic treatment, but Gibbs energy
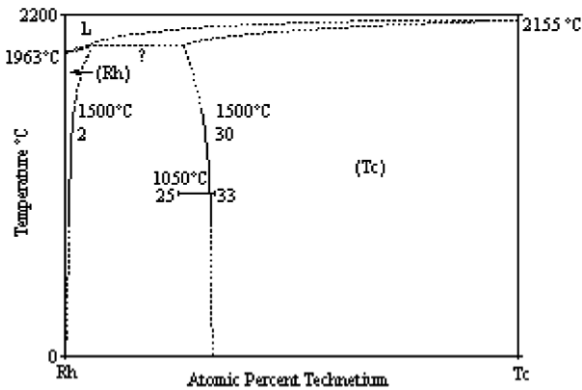
Fig. 12. Rh–Tc equilibrium diagram [39] (used with permission).

expressions for the fcc-solid phase and cph-solid phase were developed. A tie line between the fcc-solid and the cph-solid at 1773 K, which satisfied the given data, was extended from the fcc-solid boundary at $X_{Rh} \cong 0.97$ and the cph-solid boundary at $X_{Rh} \cong 0.70$. At 1323 K another tie line, which satisfied the data, was extended from the fcc-solid boundary at $X_{Rh} \cong 0.98$ and the cph-solid boundary at $X_{Rh} \cong 0.33$. From this information four independent equations were constructed that equated partial Gibbs energies for each of the elements along these tie lines; the procedure is the same in concept as that described for the Pd–Tc system. A comparison of the current treatment with the experimental work of Darby et al. [37] and Niemiec [38] is shown in Fig. 13. The diagram accommodates the limited experimental work. The position of the two phase
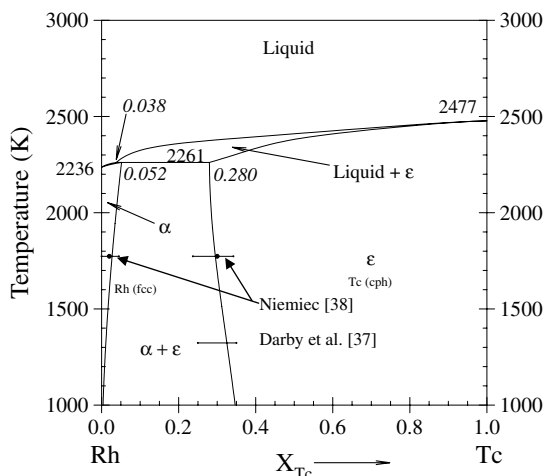
Fig. 13. The Rh–Tc system as computed in this work. Comparison of the treatment with the experimental work of Darby et al. [37] and Niemiec [38] is also shown.
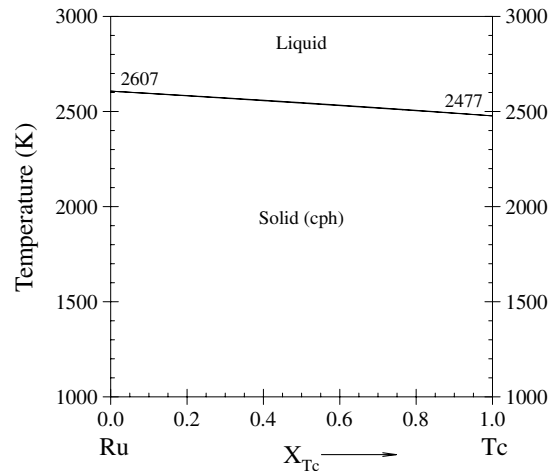

Fig. 14. The Ru–Tc system as computed in this work.

region at 1323 K suggested by Darby et al. [37] is satisfied. Furthermore, the boundaries proposed by Niemiec [38] at 1773 K are respected. The excess Gibbs energies for the solution phases are given in Table 3.

2.2.5. Ru–Tc

Darby et al. [35], using X-ray diffraction on a series of alloys previously annealed at 973 K, determined that there was a continuous series of solid cph solutions in this binary system. These results do not preclude the possibility of a solid state miscibility gap at lower temperatures, much like the Pd–Rh binary system [25,54]. However, for the purposes of this work, and in the absence of any other data, an ideal solution was assumed. The computed diagram is shown in Fig. 14.

3. The quinary model

An interpolation method was used to estimate Gibbs energies for each of the multi-component phases based upon the treatment for the binary metal combinations, discussed previously. While there are several different interpolation schemes for modelling a multi-component system from its constituent binary systems [55], the Kohler interpolation method that has been successfully applied to many other metallic systems was utilized for this work [56]. This methodology proportionally weights the influence of each binary system as shown in Eq. (23), for a ternary solution of components A, B, and C. In this equation G^E_{A-B}, for example, is the excess Gibbs energy of the *binary* mixture of A and B, at

the molar proportions of A and B (i.e., X_A and X_B) for the ternary composition to which G^E applies. The methodology is easily extended to higher order systems.

$$G^E = (X_A + X_B)^2 G_{A-B}^E + (X_A + X_C)^2 G_{A-C}^E$$
$$+ (X_B + X_C)^2 G_{B-C}^E + \ldots \quad (23)$$

The form of the interpolation scheme for the excess Gibbs energy is consistent with regular solution behaviour of each component dissolved in a solvent involving a fixed proportion of the other two components. This methodology has been found suitable in many cases as a predictive approach to provide ternary excess solution property estimates, when experimental data do not exist. As experimental data are gathered for the system, departure terms may be added to the basic interpolation. These terms take the form of products of all mole fractions raised to different powers multiplied by a temperature dependent coefficient. The correction terms vanish in the binary sub-systems.

The use of Eq. (23) requires a knowledge of the excess Gibbs energies in each binary system for all possible phases including those that may not appear in that binary system. To clarify, the cph phase does not appear in the Pd–Rh system. However, a numerical knowledge of the excess Gibbs energy of hypothetical cph-Pd and hypothetical cph-Rh is necessary. This expression amounts to an adjustable feature in the treatment of a ternary system involving a cph-phase, in which Pd and Rh are components (e.g., the Pd–Rh–Ru ternary system).

The introduction of such hypothetical Gibbs energy curves into the binary systems must not, of course, disturb the original binary treatment. That is to say, for example, the Gibbs energy of mixing equation for cph phase in the Pd–Rh binary system must at all temperatures lie above the Gibbs energy of mixing for the more stable phases (e.g., fcc-solid or liquid). An assumption of ideal mixing behaviour (i.e., $G^E = 0$) for the cph solid along with using the

hypothetical lattice parameters for cph-Pd and cph-Rh as given in Table 1, would lead to the cph phase being erroneously stable at high temperatures. There are comparable situations for the body centered cubic (bcc) in the Pd–Rh and Pd–Ru systems. To avoid these unwanted occurrences, positive mixing terms for the hypothetical cph-solid in the Pd–Rh system and for the hypothetical bcc-solid in the Pd–Rh and Pd–Ru systems were incorporated as shown in Table 2. The preceding makes clear that the evaluation of each binary system, as discussed above, cannot be done in isolation. This is an important matter that is easily overlooked and must not be underestimated when considering the binary treatments individually.

With all of the foregoing, for the ten binary sub-systems, the thermodynamic data can be divided into three parts: the lattice stabilities for the components; the excess properties of mixing for every condensed phase in each of the binary systems; and Gibbs energies for any stoichiometric phases. The lattice stabilities, G°, for each of the five components in the Mo–Pd–Rh–Ru–Tc quinary, are presented in Table 1. In all cases the liquid phase was used as the reference phase. In the quinary model, the tetragonal phase, present in the Mo–Tc system, was not extended into the multi-component system because of a lack of experimental evidence. The excess properties of mixing for the binary systems are presented in Tables 2 and 3. Finally, the properties for the four compounds, (i.e., MoRh, MoRh₃, Mo₅Ru₃, and Mo₉Tc₁₁), presented earlier in the text, are summarized in Table 7.

3.1. Comparison of thermodynamic treatment with multi-component systems

Comparison of the treatment with experimental data from Kernforschungszentrum Karlsruhe (Germany), Nagoya University (Japan), University of Birmingham (UK), and Harwell (UK), is detailed in the following sections.

Table 7
Gibbs energy of formation of the four compounds in the quinary system

Compound	Gibbs energy of formation (J mol^{-1})	Basis	Components
MoRh	$\Delta G_{MoRh}^\circ = -47100 + 16.7477T$	per 1/2 mol of MoRh	Mo$_{(liq)}$, Rh$_{(liq)}$
MoRh₃	$\Delta G_{MoRh_3}^\circ = -50339.2 + 20\,T$	per 1/4 mol of MoRh₃	Mo$_{(liq)}$, Rh$_{(liq)}$
Mo₅Ru₃	$\Delta G_{Mo_5Ru_3}^\circ = 4430 - 7.68495\,T$	per 1/8 mol of Mo₅Ru₃	Mo$_{(bcc)}$, Ru$_{(cph)}$
Mo₉Tc₁₁	$\Delta G_{Mo_9Tc_{11}}^\circ = -42794.3 + 13.8253\,T$	per 1/20 mol Mo₉Tc₁₁	Mo$_{(liq)}$, Tc$_{(liq)}$

3.1.1. The Mo–Pd–Rh–Ru sub-system

Paschoal et al. [41] have presented an extensive collection of data, derived from metallographic examination, X-ray diffraction, and electronprobe microanalysis (EPMA), for ternary and quaternary alloys in the Mo–Pd–Rh–Ru system at 1973 K.

In order to bring the computations and these experimental data into agreement, a departure term was added to Eq. (23) for the various solid solution phases as shown in Table 8. The Mo–Pd–Rh phase diagram calculated with the ternary excess parameters listed in Table 8 is shown in Fig. 15 in relation to phases determined by Paschoal et al. [41].

The Pd–Rh–Ru phase diagram using ternary departure terms added to Eq. (23) is shown in Fig. 16. There is good agreement with experimentally determined phase combinations [41].

The computed Mo–Rh–Ru and Mo–Pd–Ru ternary phase diagrams are shown in Figs. 17 and 18, respectively. In both these diagrams there are two

Table 8
Ternary excess energy terms for the liquid, fcc, bcc, and cph phases

Phase	Components	Ternary excess Gibbs energy term ($J\ mol^{-1}$)
Liquid	Mo, Pd, Rh	$G^E_{Liquid} = X_{Mo} X^2_{Pd} X_{Rh}(-9000)$
Liquid	Pd, Rh, Ru	$G^E_{Liquid} = X_{Pd} X_{Rh} X_{Ru}(-52\,500)$
bcc-solid	Mo, Pd, Rh	$G^E_{bcc} = X_{Mo} X_{Pd} X_{Rh}(-19\,730 + 10T)$
bcc-solid	Mo, Pd, Ru	$G^E_{bcc} = X_{Mo} X_{Pd} X_{Ru}(40\,000)$
bcc-solid	Mo, Rh, Ru	$G^E_{bcc} = X_{Mo} X_{Rh} X_{Ru}(-48\,000)$
cph-solid	Mo, Pd, Ru	$G^E_{cph} = X_{Mo} X_{Pd} X_{Ru}(-15\,000) + X^2_{Mo} X_{Pd} X_{Ru}(-130\,000)$
cph-solid	Mo, Pd, Rh	$G^E_{cph} = X_{Mo} X_{Pd} X_{Rh}(-89\,730 + 10T)$
cph-solid	Pd, Rh, Ru	$G^E_{cph} = X_{Pd} X_{Rh} X_{Ru}(-90\,000)$
fcc-solid	Mo, Pd, Rh	$G^E_{fcc} = X_{Mo} X_{Pd} X_{Rh}(-197\,300 + 100T)$
fcc-solid	Mo, Pd, Ru	$G^E_{fcc} = X_{Mo} X_{Pd} X_{Ru}(-115,507 + 9T)$
fcc-solid	Pd, Rh, Ru	$G^E_{fcc} = X_{Pd} X_{Rh} X_{Ru}(-40\,000)$
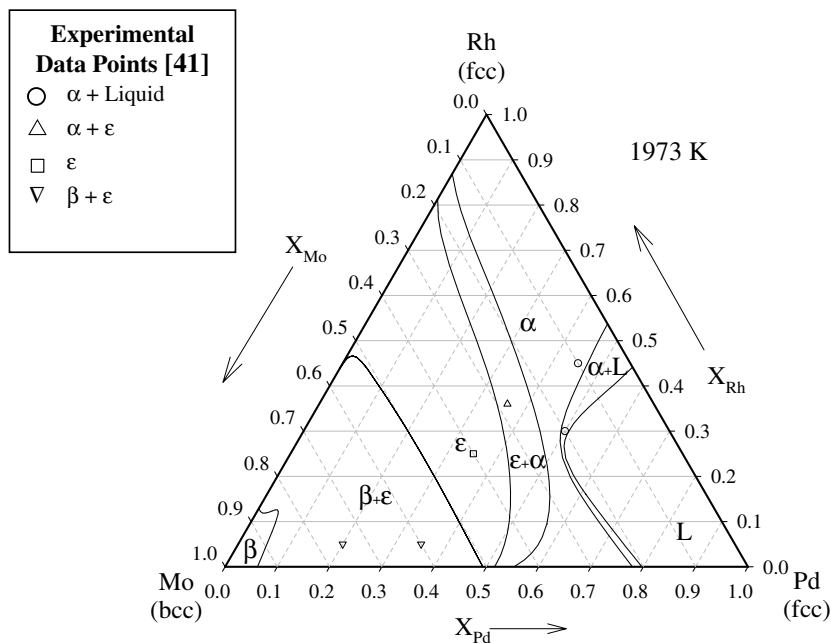
Fig. 15. Mo–Pd–Rh. *Note:* α = fcc; β = bcc; ε = cph; and L = Liquid.
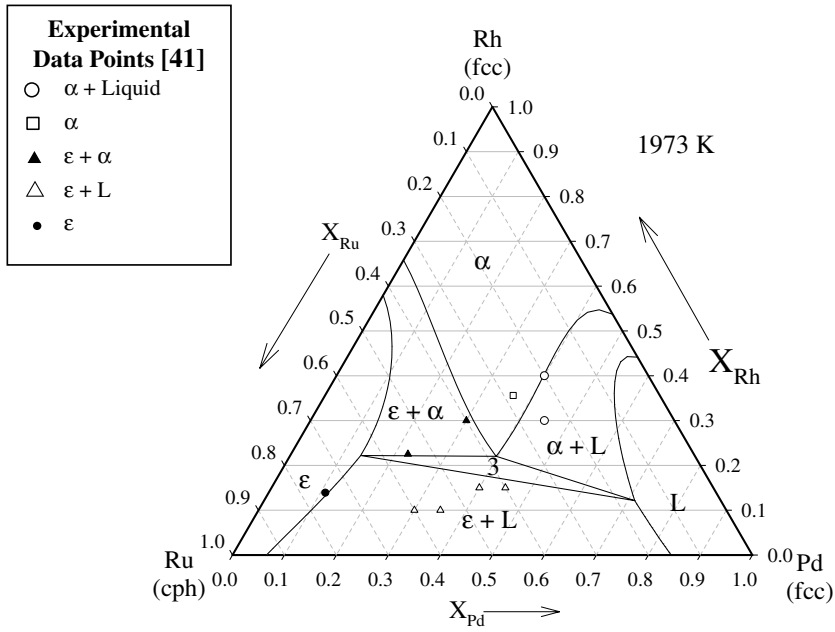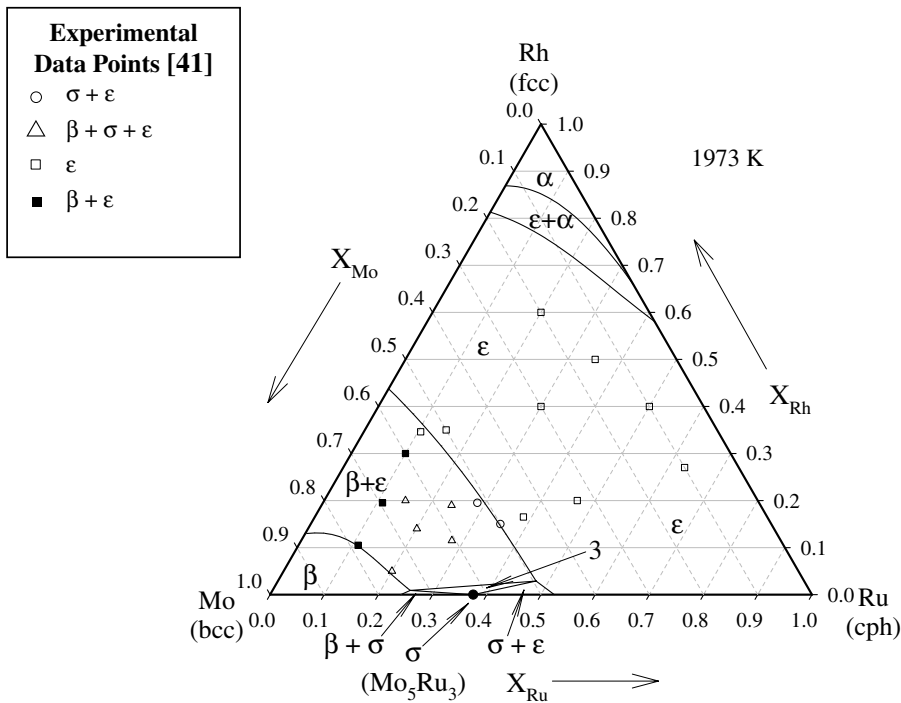
Fig. 16. Pd–Rh–Ru. *Note:* α = fcc; ε = cph; and L = liquid.

Fig. 17. Mo–Rh–Ru. *Note:* α = fcc; β = bcc; ε = cph; and σ = tetragonal.

distinct regions: the region that extends from the central ε-solid phase to the right binary edge (either Rh–Ru or Pd–Ru); and the region that lies between the β-solid phase and the ε-solid phase. For the

region that extends from the central ε-solid phase to the right binary edge, the agreement between the model and the experimental data is good. Discrepancies occur in the region that lies between the
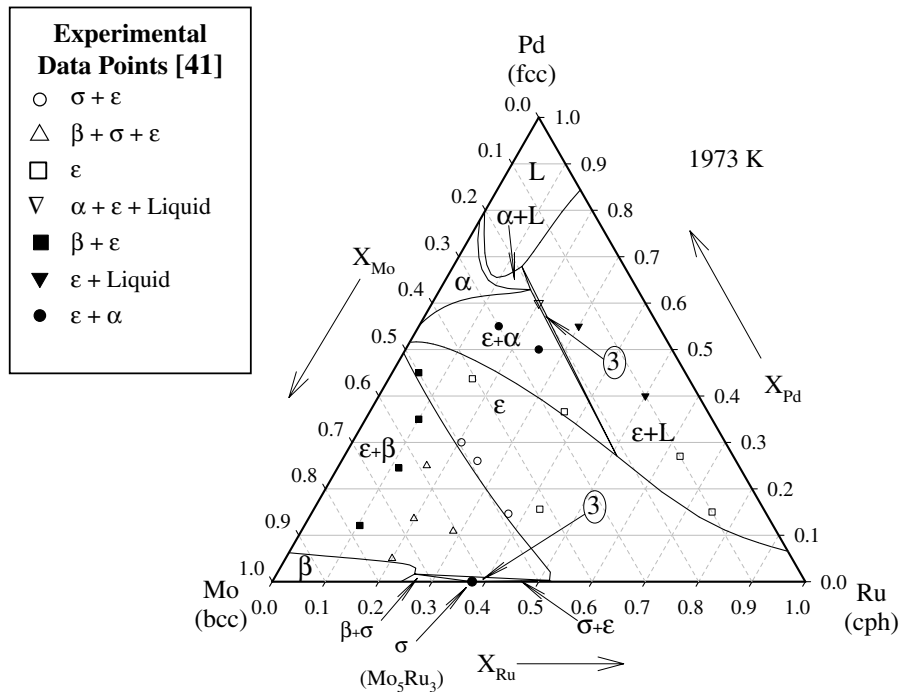
Fig. 18. Mo–Pd–Ru. *Note:* α = fcc; β = bcc; ε = cph; σ = tetragonal; L = liquid.

β-solid and ε-solid phases, where the σ-solid phase is involved. Because the model treats Mo_5Ru_3 (σ-solid) as a stoichiometric line compound, there is little flexibility to allow for the existence of σ-solid as a distinct phase region that can extend into the interior of the ternary diagram.

3.1.2. The Mo–Pd–Ru sub-system

Naito et al. [42] investigated the Mo–Pd–Ru ternary phase diagram using microscopy, X-ray diffraction, and vapour pressure measurements using a Knudsen cell coupled to a mass spectrometer. The results of their investigation are shown in Fig. 19. It should be noted that there are problems with this diagram along the Mo–Pd binary edge. It can be seen that the accepted diagram for the Mo–Pd system [23,39], clearly indicates that an ε-solid phase exists around $X_{Mo} = 50$ at.%. This means that the phase labelled α + β is questionable, as is the three phase region labelled ε + α + β.

At 1723 K, the Mo–Pd–Ru diagram, which includes Kohler interpolation departure terms is shown in Fig. 20. There is excellent agreement with the experimental results of Naito et al. [42]. The two tie lines suggested by Naito et al. [42], labelled $A_α$–$A_ε$ and $C_α$–$C_ε$, are well replicated. In fact there are only four ε-solid phase data points, indicated by a

filled circle in Fig. 20, that do not lie within the ε-solid phase region. However, the three ε-solid phase points along the $X_{Mo} = 50\%$ line, are close to the phase boundary. The fourth point, along the Pd–Ru edge, represents a graphical contradiction within the work of Naito et al. [42]. On their diagram the point $A_ε$ is at $X_{Mo} = 16.1\%$, $X_{Pd} = 17.3\%$, and $X_{Ru} = 66.7\%$, which should be between the erroneous point and the Mo–Ru edge.[2]

3.1.3. The Mo–Pd–Rh sub-system

Gürler and Pratt [43] annealed sixteen alloys in the Mo–Pd–Rh system, and studied the phase assemblages of each using optical microscopy, X-ray diffraction, SEM, and electron probe microanalysis. The results of their experimental work [43] were compared with the thermodynamic model for this ternary system at 1373 K, shown in Fig. 21. It should be pointed out that the compound MoRh₃, which is stable to 1470 K in the binary system, was withdrawn from the analysis to facilitate comparison since Gürler and Pratt [43] did not consider it.

---

[2] In Fig. 19 $A_ε$ is positioned above the $X_{Pd} = 20\%$, which permits the diagram to be drawn to include the debatable point within the ε-solid phase region.
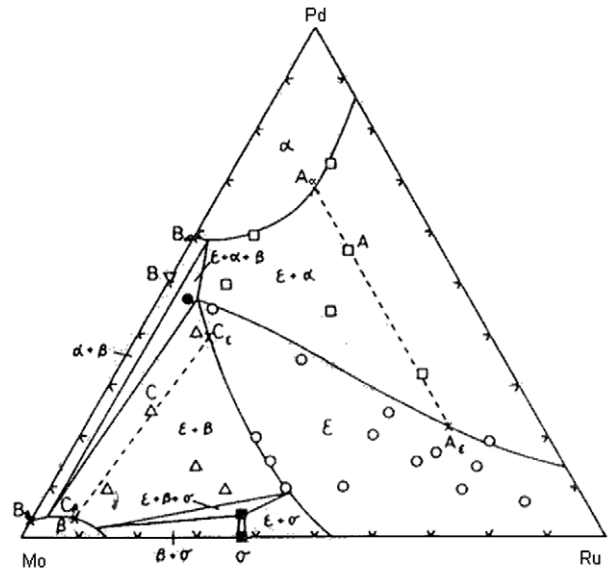
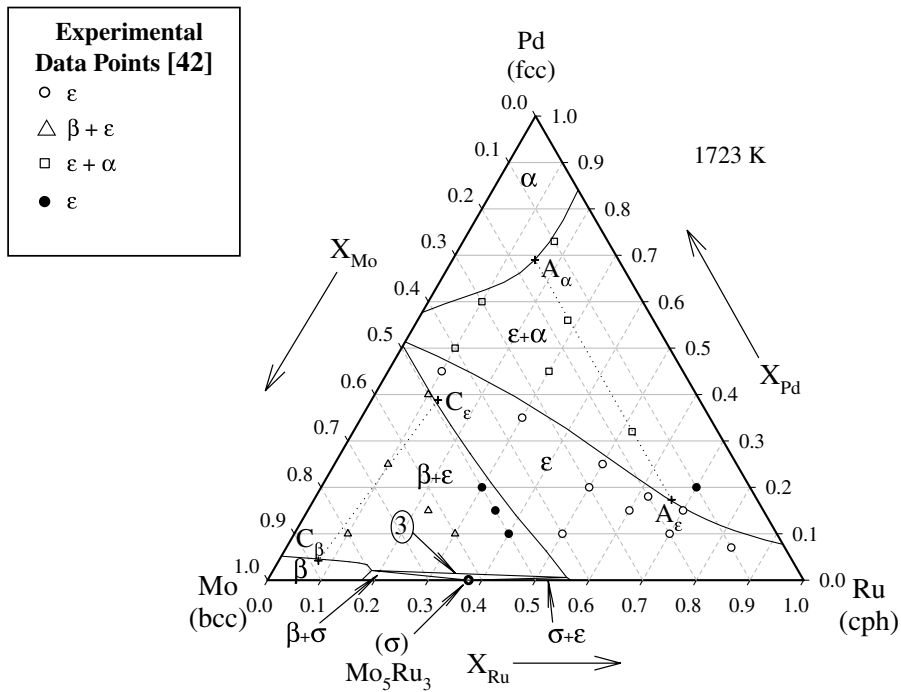Fig. 19. The Mo–Pd–Ru diagram at 1723 K, by Naito et al. [42] (used with permission).

Fig. 20. Comparison of the experimental data from Naito et al. [42] to the proposed Mo–Pd–Ru diagram. *Note:* α = fcc; β = bcc; ε = cph; and σ = tetragonal.

Gürler and Pratt used their experimental data to develop a computer calculation of the Mo–Pd–Rh ternary phase diagram [44]. Their evaluation at 1373 K is shown in Fig. 22. Fig. 21 appears to better
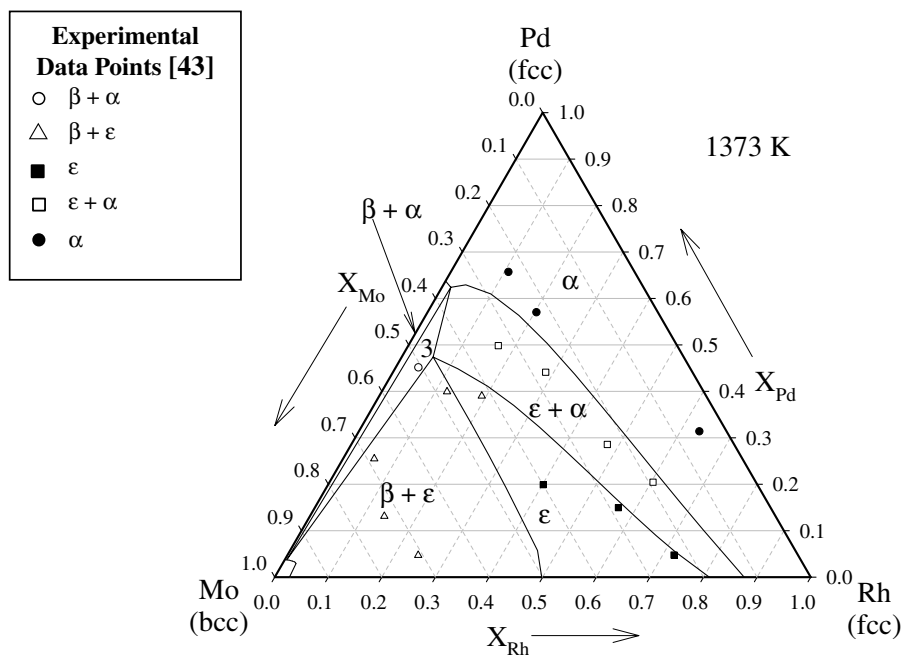
Fig. 21. Mo–Pd–Rh. The experimentally determined points are from Gürler and Pratt [43], with MoRh$_3$ suppressed in the calculation to facilitate comparison. *Note:* α = fcc; β = bcc; and ε = cph.

represent the experimental data in the central region of the diagram. A copy of the figure from the paper by Gürler and Pratt [44], which shows the experimental data, is shown in Fig. 23.

3.1.4. The Mo-Pd-Tc sub-system

Haines et al. [45] are the only researchers to propose ternary phase diagrams that involve Tc in combination with pairs of elements from amongst the noble metals. The methodology that Haines et al. employed is similar to that used in this work, that is, building upwards from binary evaluations. However, it is clear from the diagrams of Mo-Tc, Pd-Tc, and Rh-Tc (see previous sections) that their proposed models do not fit the limited experimental data that exist for these binary systems. The ternary phase diagram (Fig. 24) predicted by the current thermodynamic treatment for Mo–Pd–Tc is shown in Fig. 25. Note that Fig. 25 includes the tetragonal σ-phase and the compound Mo$_9$Tc$_{11}$.

4. Quinary solution model applied to metallic inclusion prediction in fuel

A typical equilibrium calculation for reactor fuel of differing burnup has been performed using the noble metal treatment developed here in conjunction with thermodynamic treatments for the UO$_2$ fuel, solute oxides, and other possible phases [15]. For various degrees of fuel burnup, the initial elemental fuel inventory was calculated using the ORIGEN2 code [57]. Gibbs energy minimization methods incorporated into computational software [58] then determine the predicted phase assemblage for a specified system pressure (e.g., 1 atm) and temperature (e.g., 1500 and 2000 K). Partial results from four such calculations are summarized in Table 9, for fuel burnups[3] of 35 MWh (kgU)$^{-1}$ and 175 MWh (kgU)$^{-1}$.

It can be seen that for irradiated fuel at higher temperatures, the noble metals, as expected form a cph-solid phase [12,21]. However, for lower burnups

---

[3] Partial inventories, based on the ORIGEN2 code, are included here so that the reader can appreciate the differences between a low burnup situation, 35 MWh (kgU)$^{-1}$, and a higher burnup, 175 MWh (kgU)$^{-1}$. In both cases, the original inventory of oxygen in the fuel, calculated as that associated with pure UO$_2$, remains constant regardless of burnup.

For a burnup of 35 MWh (kgU)$^{-1}$, the fuel, originally 100% UO$_2$, has changed through fission of uranium, to have a metal and/or fission product inventory of: 99.5688% U, 0.1062% Pu, 0.0456% Zr, 0.0289% Mo, 0.0252%Ru, 0.0082% Tc, 0.0044% Pd, 0.0013% Rh, etc.

For a burnup of 175 MWh (kgU)$^{-1}$, the metal and/or fission product inventory becomes: 98.0593% U, 0.3647% Pu, 0.2051% Zr, 0.1544% Mo, 0.1422%Ru, 0.0459% Tc, 0.0494% Pd, 0.0203% Rh, etc.
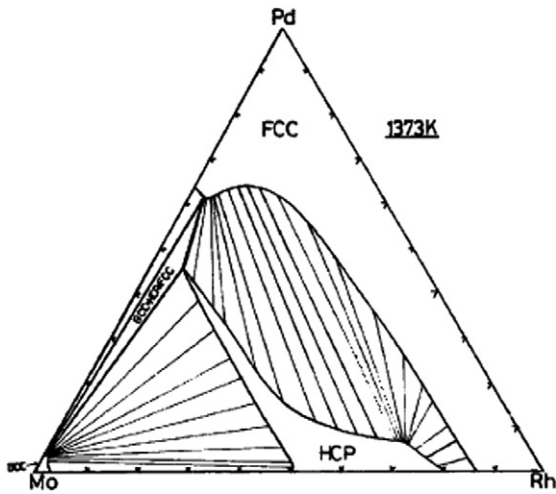
Fig. 22. Mo–Pd–Rh at 1373 K computed by Gürler and Pratt [44] (used with permission).

Fig. 24. Mo–Rh–Tc from Haines et al. [45]. *Note:* α = fcc; β = bcc; ε = cph (used with permission).

and at lower temperatures, the presence of the bcc-solid phase, in addition to the cph-solid may be possible. This may be a consequence of the fraction Mo to total noble metals decreasing from 42.5% to 37.5% (i.e., moving away from the bcc region associated with bcc-Mo, and towards the dominant cph-solid region) as burnup increases.
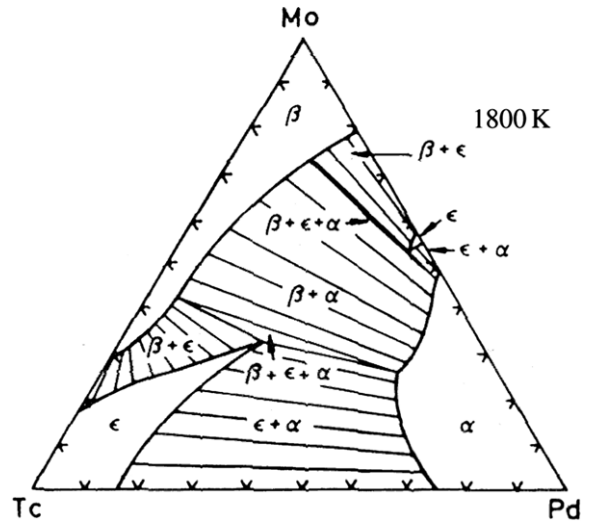
A further consequence of the quinary model is that the oxidation behaviour of Mo can be represented. In particular the distribution of Mo between that dissolved in the UO_2 and that dissolved in the noble metal phase(s) can be computed from the equilibrium:
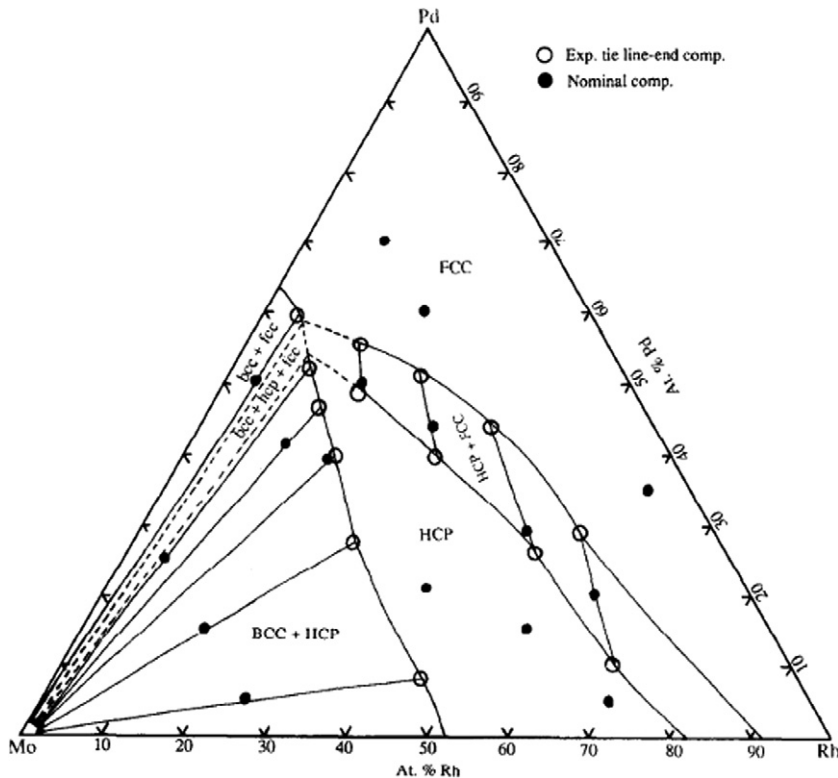

Fig. 23. Mo–Pd–Rh at 1373 K from Gürler and Pratt [43] (used with permission).
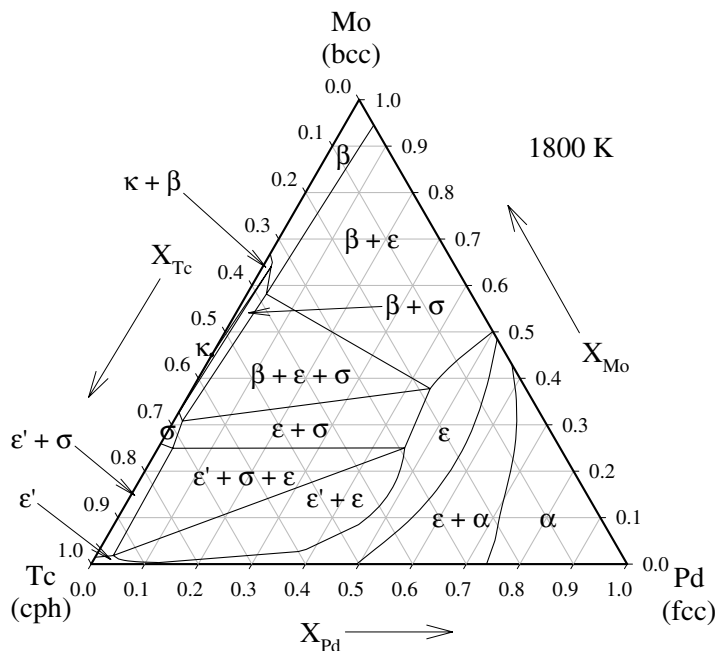
Fig. 25. The Mo–Pd–Tc diagram predicted by the thermodynamic treatment. *Note:* α = fcc; β = bcc; ε = cph; ε' = cph; σ = tetragonal; and $\kappa = Mo_9Tc_{11}$.

Table 9
Results from four equilibrium computations, showing predicted metallic inclusion phases, the associated activity of Mo, MoO_2 (both with respect to the pure solid), and P_{O_2}

Fuel burnup MWh (kgU)$^{-1}$	T (K)	cph-solid Phase fraction	bcc-solid (atomic %)	a_{Mo}[a]	a_{MoO_2}[a]	P_{O_2} (atm)
35	1500	76.6	23.4	0.689	2.604×10^{-6}	2.54×10^{-17}
35	2000	100%	0%	0.560	6.513×10^{-6}	5.98×10^{-12}
175	1500	100%	0%	0.067	3.787×10^{-5}	3.79×10^{-15}
175	2000	100%	0%	0.003	1.386×10^{-4}	2.64×10^{-8}

[a] With respect to the pure solid.

$$Mo_{(s)} + O_{2(g)} \rightleftharpoons MoO_{2(dissolved)} \qquad (24)$$

This implies that the distribution of Mo can provide the oxygen partial pressure associated with partially burned fuel. Of course to do this, the activity of Mo, as provided by the current treatment, is essential. There are many other collateral benefits to treating multi-component phase equilibrium in the manner described above.

5. Conclusions

A thermodynamic treatment for the complete Mo–Pd–Rh–Ru–Tc quinary system, of interest in understanding metallic inclusions in nuclear fuel, was constructed on a foundation of the 10 binary sub-systems. The Kohler interpolation method, with the inclusion of a limited number of ternary departure terms, has been demonstrated to fit most of the direct observations of the coexisting phase combinations. The treatment is particularly valuable when combined with thermodynamic models and data for the other phases present in nuclear fuel which make possible computations of overall phase equilibrium by Gibbs energy minimization methods [15]. Such a computation predicts, from first principles, a hexagonal phase for the noble metal inclusion as observed by O'Boyle [12].

References

[1] C.M. Allison, G.A. Berna, L.J. Siefken, SCDAP/MOD1 Theory and Models, FIN No. A6360: Idaho National Engineering Laboratory, January 1985.

[2] A.B. Reynolds, J.L. Kelley, S.T. Kim, Nucl. Technol. 74 (1986) 76.

[3] W.J. Camp, M.F. Young, J.L. Tomkins, J.E. Kelly, P.J. Maudlin, R.J. Henninger, MELPROG-PWR/MODO: A Mechanistic Code for Analysis of Reactor Core Melt Progression and Vessel Attack Under Severe Accident Conditions, NUREG/CR-4909 SAND85-0237 R3: Sandia National Laboratories, April 1987.

[4] D. Cubicciotti, J. Nucl. Mater. 154 (1988) 53.

[5] M. Ramamurthi, M.R. Kuhlman, Refinement of CORSOR – An Empirical In-Vessel Fission Product Release Model, Battelle report, US Nuclear Regulatory Commission, October 1990.

[6] M. Gardani, C. Ronchi, J. Nucl. Mater. 107 (1991) 315.

[7] M.F. Osborne, R.A. Lorenz, Nucl. Saf. 33 (1992) 344.

[8] B. André, G. Ducros, J.P. Lévêque, M.F. Osborne, R.A. Lorenz, D. Maro, Nucl. Technol. 114 (1996) 23.

[9] B.J. Lewis, B.J. Corse, W.T. Thompson, M.H. Kaye, F.C. Iglesias, P. Elder, R. Dickson, Z. Liu, J. Nucl. Mater. 252 (1998) 235.

[10] F.C. Iglesias, B.J. Lewis, P.J. Reid, P. Elder, J. Nucl. Mater. 270 (1999) 21.

[11] J.I. Bramman, R.M. Sharpe, D. Thom, G. Yates, J. Nucl. Mater. 25 (1968) 201.

[12] D.R. O'Boyle, F.L. Brown, A.E. Dwight, J. Nucl. Mater. 35 (1970) 257.

[13] D.R. Olander, in: Fundamental Aspects of Nuclear Reactor Fuel Elements, 1976, p. 172, Chapter 12.

[14] B.J. Lewis, W.T. Thompson, F. Akbari, D.M. Thompson, C. Thurgood, J. Higgs, J. Nucl. Mater. 328 (2004) 180.

[15] M.H. Kaye, C. Morrison, J.D. Higgs, F. Akbari, B.J. Lewis, W.T. Thompson, First principles model of CANDU fuel phase equilibrium, in: 9th International Conference on CANDU Fuel, Belleville, Ontario, 18–21 September 2005.

[16] J.H. Davies, F.T. Ewart, J. Nucl. Mater. 41 (1971) 143.

[17] G. Giacchetti, C. Sari, Nucl. Technol. 31 (1976) 62.

[18] H. Kleykamp, J. Nucl. Mater. 84 (1979) 109.

[19] T. Matsui, T. Hoshikawa, K. Naito, Solid State Ionics 40&41 (1990) 996.

[20] T. Matsui, K. Naito, Thermochim. Acta 139 (1989) 299.

[21] H. Kleykamp, J.O.A. Paschoal, R. Pejsa, F. Thümmler, J. Nucl. Mater. 130 (1985) 426.

[22] A.E. Dwight, D.R. O'Boyle, J. Nucl. Mater. 136 (1985) 280.

[23] R. Gürler, J. Alloys Compd. 191 (1993) 83.

[24] R. Gürler, J.N. Pratt, J. Alloys Compd. 189 (1992) 97.

[25] R. Gürler, L.A. Cornish, J.N. Pratt, J. Alloys Compd. 191 (1993) 165.

[26] R. Gürler, J. Alloys Compd. 191 (1993) 31.

[27] E. Anderson, W. Hume-Rothery, J. Less-Common Metal 2 (1960) 443.

[28] B.F. Kieffer, K. Sedlatschek, in: Symposium on High-Temperature Refractory Metals, Gordon and Breach Science Publishers, NY, 1969, p. 441.

[29] H. Kleykamp, J. Nucl. Mater. 167 (1989) 49.

[30] H. Kleykamp, J. Less-Common Met. 136 (1988) 271.

[31] H. Kleykamp, J. Less-Common Met. 144 (1988) 79.

[32] M.H. Rand, P.E. Potter, Physica 103B (1981) 21.

[33] V.B. Compton, E. Corenzwit, J.P. Maita, B.T. Matthias, F.J. Morin, Phys. Rev. 123 (5) (1961) 1567.

[34] J.B. Darby Jr., S.T. Zegler, Phys. Chem. Solids 23 (1962) 1825.

[35] J.B. Darby Jr., D.J. Lam, L.J. Norton, J.W. Downey, J. Less-Common Met. 4 (1962) 558.

[36] N.V. Ageev, C.V. Kopetskii, E.M. Savitskii, V.S. Shekhtman, Doklady Akad. Nauk. S.S.S.R. 129 (1959) 87.

[37] J.B. Darby Jr., L.J. Norton, J.W. Downey, J. Less-Common Met. 5 (1963) 397.

[38] J. Niemiec, Bull. de L'Académie Polonaise Des Sci. 11 (12) (1963) 665.

[39] T.B. MassalskiBinary Alloy Phase Diagrams, vol. 1&2, ASM, Metals Park, Ohio, 1986.

[40] E.H.P. Cordfunke, R.J.M. Konings, Thermochemical Data for Reactor Materials and Fission Products, Elsevier Science Publishers, Amsterdam, 1990.

[41] J.O.A. Paschoal, H. Kleykamp, F. Thümmler, Zeitschrift Fuer Metallkunde 74 (1983) 652.

[42] K. Naito, T. Tsuji, T. Matsui, A. Date, J. Nucl. Mater. 154 (1988) 3.

[43] R. Gürler, J.N. Pratt, J. Nucl. Mater. 186 (1991) 39.

[44] R. Gürler, J.N. Pratt, J. Nucl. Mater. 200 (1993) 16.

[45] H.R. Haines, P.E. Potter, M.H. Rand, in: Proceedings of an IAEA Symposium on Thermodynamics of Nuclear Materials, vol. 1, 1979, p. 471.

[46] M.H. Kaye, A Thermodynamic Model for Noble Metal Alloy Inclusions in Nuclear Fuel Rods and Application to the Study of Loss-of-Coolant Accidents, Doctoral thesis, Queen's University, 2001.

[47] K.T. Jacob, S. Priya, Y. Waseda, J. Phase Equilib. 19 (4) (1998) 340.

[48] E. Raub, J. Less-Common Met. 1 (1959) 3.

[49] E. Raub, H. Beeskow, D. Menzel, Zeitschrift Fuer Metallkunde 50 (1959) 428.

[50] J.E. Shield, R.K. Williams, Scripta Metall. 21 (11) (1987) 1475.

[51] R. Gürler, J. Alloys Compd. 285 (1999) 133.

[52] L. Brewer, in: O. Kubaschewski (Ed.), Atomic Energy Review Special Issue No. 7, IAEA, Vienna, 1980.

[53] D.R. Gaskell, Introduction to Metallurgical Thermodynamics, McGraw-Hill, NY, 1981.

[54] H. Okamoto, J. Phase Equilib. 15 (3) (1994) 369.

[55] P. Chartrand, A.D. Pelton, J. Phase Equilib. 21 (2) (2000) 141.

[56] F. Kohler, Monatshefte Für Chemie 91 (1960) 738.

[57] A.G. Croff, ORIGEN2 – A Revised and Updated Version of the Oak Ridge Isotope Generation and Depletion Code, Report ORNL-5621, July 1980.

[58] C.W. Bale, A.D. Pelton, W.T. Thompson. Facility for the Analysis of Chemical Thermodynamics, Ecole Polytechnique de Montreal/McGill University.